Hindawi
Journal of Advanced Transportation
Volume 2020, Article ID 9181836, 11 pages
https://doi.org/10.1155/2020/9181836

Research Article

Analysis of V2V Messages for Car-Following Behavior with the Traffic Jerk Effect

Tenglong Li,[1,2] Fei Hui ,[1,2] Ce Liu,[1] Xiangmo Zhao ,[1,2] and Asad J. Khattak[1,3]

[1]*School of Information Engineering, Chang'an University, Xi'an 710064, China*
[2]*The Joint Laboratory for Internet of Vehicles, Ministry of Education-China Mobile Communications Corporation, Chang'an University, Xi'an 710064, China*
[3]*Department of Civil and Environmental Engineering, University of Tennessee, Knoxville, TN 37996, USA*

Correspondence should be addressed to Fei Hui; feihui@chd.edu.cn

Received 15 May 2019; Revised 13 October 2019; Accepted 14 November 2019; Published 20 January 2020

Academic Editor: Eneko Osaba

The existing model of sudden acceleration changes, referred to as the traffic jerk effect, is mostly based on theoretical hypotheses, and previous research has mainly focused on traditional traffic flow. To this end, this paper investigates the change in the traffic jerk effect between inactive and active vehicle-to-vehicle (V2V) communications based on field experimental data. Data mining results show that the correlation between the jerk effect and the driving behavior increases by 50.6% on average when V2V messages are received. In light of the data analysis results, a new car-following model is proposed to explore the jerk effect in a connected environment. The model parameters are calibrated, and the results show that the standard deviation between the new model simulation data and the observed data decreases by 38.2% compared to that of the full velocity difference (FVD) model. Linear and nonlinear analyses of the calibrated model are then carried out to evaluate the connected traffic flow stability. Finally, the theoretical analysis is verified by simulation experiments. Both the theoretical and simulation results show that the headway amplitude and velocity fluctuations are reduced when considering the jerk effect in a connected environment, and the traffic flow stability is improved.

1. Introduction

As the basis of microscopic traffic flow, the car-following model [1, 2] is used to describe the motion characteristics of a vehicle that follows another vehicle. This situation is the most common driving behavior in single-lane traffic flow [3–5]. In the past, notable efforts have been made to model car-following behavior [6–9]. Bando et al. [6] proposed an optimal velocity (OV) model based on the assumption that each vehicle has an optimal desired speed while driving. This model can successfully explain actual traffic phenomena, such as stop-and-go waves and congestion evolution, in a simple form. Helbing and Tilch [7] subsequently found that the OV model exhibited unrealistic acceleration and deceleration behaviors in a simulation. To overcome this drawback, a generalized force (GF) model was proposed. However, the GF model cannot describe the wave motion velocity of a vehicle in a blocking density. Thus, Jiang et al. [8] proposed a full velocity difference (FVD) model based on the GF model. This model has been widely used in traditional traffic flow modeling. The differential equation of the FVD model is:

$$a_n(t) = a\big(V(s) - v_n(t)\big) + \kappa \Delta v_n(t), \tag{1}$$

where a indicates the sensitivity coefficient of the driver's response; $V(s)$ is the OV function; s represents the headway between vehicle n; and its preceding vehicle $n+1$; $v_n(t)$ represents the velocity of vehicle n at time t; and κ is a response coefficient different from a.

With the development of connected vehicles (CVs), research on traffic flow theory has gradually evolved from traditional traffic flow modeling to connected traffic flow [10–16]. A CV can share its status (e.g., position, speed, and acceleration) with other CVs within a certain range via vehicle-to-vehicle (V2V) or vehicle-to-infrastructure (V2I) communication. Based on this feature, Li et al. [17] proposed a car-following model that accounted for the communication probability to capture the car-following behavior of CVs equipped with vehicle-to-everything (V2X) communications.

Figure 1: Field experiments. (a) Map of the experimental site. (b) Data acquisition experiments.

These researchers conducted field experiments to verify the effectiveness of the proposed method in terms of trajectory and velocity profiles. Ge et al. [18] proposed a class of connected cruise control algorithms based on human driving behavior and conducted experiments to examine the benefits of utilizing motion information from preceding vehicles. Xie et al. [19] proposed a generic car-following framework to model heterogeneous traffic and developed a driver assistance strategy for CVs. Sharma et al. [20] used prospect theory to incorporate driver compliance behavior into CV driving strategies. The results show that the new model can successfully predict the car-following dynamics of CVs. Zheng et al. [21] developed a safety rule-based cellular automaton (CA) model under a V2V environment. All these studies show that CVs can significantly improve traffic safety and energy efficiency and can also bring additional social benefits by reducing traffic flow fluctuations.

In actual traffic scenarios, vehicles often undergo sudden acceleration changes, and this effect is called traffic jerk. This kind of disturbance easily spreads upstream in traffic, resulting in phantom traffic jams [22–24]. In recent years, many scholars have studied various traffic flow models that consider traffic jerk. Redhu and Siwach [25] proposed an extended flux difference lattice hydrodynamics model by considering the traffic jerk effect. The traffic jerk effect was examined through linear and nonlinear stability analyses in that paper. Zhai and Wu [26] proposed a continuum traffic model that considered the effects of driver characteristics and traffic jerk. The simulation results showed that driver characteristics and traffic jerk effects play significant roles in traffic flow stability and emissions. Cheng et al. [27] proposed a macro traffic flow model that simultaneously considered anticipation and traffic jerk. Numerical simulations demonstrated that the proposed model could suppress traffic congestion and reduce energy consumption. Song et al. [28] developed an improved car-following model that accounted for traffic jerk and the FVD. The analytical and numerical analysis results showed that the improved model had the ability to describe the phase transition and critical phenomena in real traffic conditions. Jin et al. [29] presented an improved car-following model to explore the effects of driver memory and jerk on traffic flow. The evolution of traffic congestion and the corresponding energy consumption were then discussed. It is reasonable to conclude from the above literature that traffic jerk has a significant impact on traffic flow stability and should be considered in car-following behavior modeling.

However, most research results are derived only from theoretical hypotheses and not from field data mining analysis results. These proposed models are also not calibrated and verified through experimental data. This shortcoming will seriously affect the validity of the corresponding research results. In addition, the above-mentioned studies mainly discuss traditional traffic flow and do not include the jerk effect in connected traffic flow. It is of great significance to capture the nature of stop-and-go traffic waves [30] and the impact of V2V messages on traffic jerk by using mathematical and physical models. The spatiotemporal evolution of traffic flow can be analyzed and predicted by established models. This approach can provide reasonable transportation planning advice for traffic management centers and guide the design of human-like autonomous car-following planning algorithms [31, 32].

Therefore, this paper investigates changes in the traffic jerk effect between inactive and active V2V communication environments based on field experimental data. In light of the data analysis results, a car-following model is proposed to explore the jerk effect in a connected environment. By calibrating the parameters of the proposed model, the fitting ability of the model to real traffic scenarios is verified. The linear and nonlinear stability conditions of the calibrated model are then derived. Finally, simulation experiments are conducted to demonstrate the theoretical results.

2. Model Formulation

2.1. Experimental Setup. This paper used the car-following data of CVs previously collected by our research team (see Figure 1) [33, 34] to analyze the impact of V2V communication on the jerk effect in traffic flow (i.e., to evaluate the correlation between the jerk effect and car-following behavior in inactive and active V2V cases). The site selected for the experiment was the 2.4-km circular runway of the Chang'an University's vehicle testing field. Two CVs were used for the field experiments. The CVs were retrofitted by our research group based on the production vehicles. The retrofit equipment included an

MK5 on-board unit manufactured by Cohda Wireless for V2V communication, accelerometers, differential GPS, human-machine interface (HMI) equipment, etc. The HMI can guide and warn the driver based on his/her driving behavior through voice and interface prompts. For a more detailed introduction to our connected experimental platform, refer to [34].

The experiment process is as follows. After the leading vehicle starts, the driver is required to continuously decelerate and then accelerate again; that is, the acceleration of the leading vehicle is constantly fluctuating. The driver of the following vehicle is required to follow the leading vehicle in the same lane and is not allowed to overtake the leading vehicle. In this way, we can analyze the experimental data of the two vehicles to explore the jerk effect in traffic flow. In addition, we can analyze the influence of V2V messages on car-following behavior with the traffic jerk effect by comparing the driving behavior with inactive and active V2V communications. Because there are many factors affecting the results of traffic experiments, we conducted four repeated tests with the same test scenario to ensure that the experimental data analysis results are consistent. The experimental data include the velocity, acceleration, and position of each vehicle. The headway and velocity difference between the leading vehicle and the following vehicle can be calculated. All data acquisition frequencies were set to 20 Hz.

Notably, the dataset of the CVs used in this study is collected under homogeneous traffic flow, i.e., 100% market penetration rate (MPR) of the CVs. The driving prompt/warning strategies of the CVs are the same. In fact, the large-scale popularization of CVs will take a certain amount of time. Thus, regular vehicles and CVs will be mixed in real road environments. In addition, the driving strategy should be adjusted according to the MPR of the CVs and the vehicular order sequence to improve the safety, stability, and throughput of traffic flow. Experimental data acquisition and modeling analyses of heterogeneous platoons with V2V communication will be carried out in our future work.

2.2. Data Mining Analysis. In the literature review section, we find that previous studies have concluded based on theoretical analyses and numerical simulations that traffic jerk has a significant impact on traffic flow stability and should be considered in car-following behavior modeling. However, this conclusion has not been verified by field tests. Therefore, we used the experimental data to explore the correlation between traffic jerk and car-following behavior. In addition, previous theoretical studies suggested that the driving stability of CVs will be smoother than that of regular vehicles (RVs), as a CV can accurately obtain the driving information of neighboring vehicles [12, 13]. Thus, the changes between the jerk effect and driving behavior under active and inactive V2V communications should be compared through correlation analysis.

Correlation analysis is the analysis of two or more related variables to measure the closeness of the two variables. To explore the effect of V2V information on the correlation between jerk and car-following behavior, the maximal information coefficient (MIC) [35] is used in this paper to measure the degree of linear or nonlinear similarity between two variables. The higher the degree of similarity, the greater the value. The calculation formula is as follows:

$$\mathrm{MIC}[x; y] = \max_{|X||Y|<B} \frac{I[X; Y]}{\log_2(\min(|X|, |Y|))}, \tag{2}$$

where $I[X; Y] = \sum_{X,Y} p(X, Y)\log_2 p(X, Y)/p(X)p(Y)$; $p(X, Y)$ is the joint probability density distribution function and B is a function of sample size. X and Y are the variables studied and represent the acceleration of the following vehicle and the jerk effect, respectively. The correlation analysis results are presented in Table 1.

Table 1: Correlation analysis results.

Experiment no.	Sample size	MIC (inactive V2V)	MIC (active V2V)
1	708	0.124	0.352
2	1027	0.207	0.213
3	603	0.141	0.154
4	284	0.222	0.301
5	860	0.135	0.230
Mean	—	0.166	0.250

Previous studies of traditional traffic flows have concluded that traffic congestion can be efficiently suppressed by considering the impact of jerk. More specifically, a driver's avoidance of unnecessary jerk can obviously stabilize traffic flow [25–28]. The data analysis results in Table 1 further indicate that the correlation between the jerk effect and driving behavior increases by 50.6% on average compared to that of an RV since V2V communication technology provides instant information regarding the interactions between vehicles [33, 36, 37]. This finding may improve the stability of connected traffic flow. This conjecture based on data mining analysis results is verified via mathematical modeling and theoretical stability analysis.

2.3. New Model. According to the above-mentioned data analysis results, a car-following model is extended based on the FVD model to describe the jerk effect in connected traffic flow; this model is referred to as FVD-JC, and it is expressed as follows:

$$a_n(t) = a\big(V(s) - v_n(t)\big) + \kappa\Delta v_n(t) - \big(\lambda\Theta(s_c - s) + \gamma\big)J_n(t), \tag{3}$$

where λ and γ are the jerk parameters to be calibrated; $J_n(t) = dv_n(t)/dt - dv_n(t-1)/dt$; Θ is the Heaviside function; and other parameters have the same meanings as those of the FVD model. The specific form of the OV function [7] is $V(s) = V_1 + V_2\tanh\big(C_1(s - L_c) - C_2\big)$.

2.4. Parameter Calibration. The proposed car-following model can be calibrated to verify the fitting ability of the model to observed traffic data and obtain more realistic driving behaviors in traffic simulations [38]. The calibration process is usually considered a nonlinear optimization problem [43], whose objective function is defined as follows:

$$\min_{\beta} f_v(\beta) = \frac{1}{m}\sum_{j=1}^{m}\Big[v_n^{\mathrm{sim}}(jT, \beta) - v_n^{\mathrm{obs}}(jT)\Big]^2, \tag{4}$$

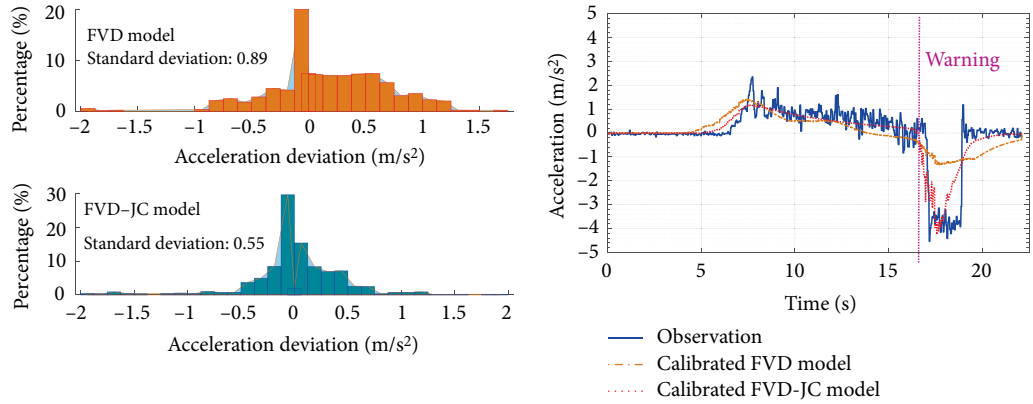

Figure 2: Comparison of the calibration results. (a) Acceleration deviation distribution. (b) Acceleration replicated by different models.

where β is a calibration parameter vector; m is the size of the dataset; j is the current simulation step size; T is the sampling time; $v_n^{\text{sim}}(\cdot)$ is the simulation velocity of the target vehicle; and $v_n^{\text{obs}}(\cdot)$ is the observed velocity.

The genetic algorithm (GA) is used to calibrate the FVD-JC model parameters. The GA toolbox of MATLAB is used in the calibration process of the car-following model. For a detailed account of the GA and a comparison of calibration algorithms, refer to [39] and the many references therein. Figure 2(a) shows that the acceleration deviation distribution of the FVD-JC model is more concentrated than that of the FVD model; e.g., the standard deviation is reduced by 38.2%. This result indicates that model improvement is effective and necessary. To intuitively explain why the fitting ability of the FVD-JC model is better than that of the FVD model, we randomly select pieces of data before and after the V2V warning information is received.

As shown in Figure 2(b), the FVD model can be fitted to the observed data when warning information is not received; however, when warning information is received, the FVD model cannot fit the actual driving behavior very well. It can be seen that the FVD-JC model fits the measured data well. As shown in Figure 3, the value of the cumulative distribution function of the FVD-JC model is larger than that of the FVD model in the smaller value area of the acceleration deviation. Thus, compared with the FVD model, the simulation error of the FVD-JC model is mainly distributed in the smaller value area. This result is consistent with that of Figure 2(a).

The calibration results indicate the necessity of our new model, as the parameters of the FVD model can no longer be adjusted to describe and fit the experimental data at this time. We need to make improvements in the model structure. These results also confirm the validity of the previous data analysis results.

In this paper, the values of the OV-related parameters are chosen from the results in [7]. The other parameters take the average values of the calibration results. Therefore, the parameters of the proposed model are finally set as follows: $a = 0.41$, $\kappa = 0.5$, $\lambda = 0.05$, $\gamma = 0.05$, $V_1 = 6.75$, $V_2 = 7.91$, $C_1 = 0.13$, and $C_2 = 1.57$.

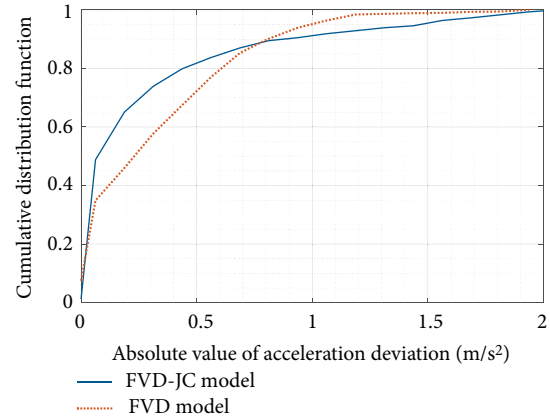

Figure 3: Cumulative distribution of the absolute value of the acceleration deviation.

3. Stability Analysis

The stability of traffic flow [40] as an indicator of spontaneous congestion patterns is an important consideration in car-following behavior modeling [42, 42]. Moreover, traffic flow stability will directly affect traffic safety, energy consumption, and throughput. Therefore, traffic flow stability can be used as an essential traffic evaluation indicator. According to the stability analysis results, we can determine the stable and unstable regions of traffic flow under different conditions and then provide guidance for suppressing traffic congestion.

3.1. Linear Stability Analysis. To analyze the ability of the proposed model against a small disturbance, we first suppose the current state of traffic flow is uniform. The OV is taken as $V(\tilde{s})$, where $\tilde{s}$ is the equilibrium headway of each vehicle in a platoon. Hence, the location of each vehicle in the steady-state solution is given as:

$$p_n^0(t) = \tilde{s}n + V(\tilde{s})t, \ \tilde{s} = L/N, \tag{5}$$

where L is the closed single-lane length and N is the total number of vehicles in the observed lane.

Then, we substitute a small disturbance $y_n(t) = e^{(ikn+zt)}$ into the uniform steady-state Equation (5) and obtain $p_n(t) = p_n^{(0)}(t) + y_n(t)$. To facilitate further derivation, we convert this result to the following equivalent form:

$$y_n(t) = p_n(t) - p_n^{(0)}(t). \tag{6}$$

The first derivative of Equation (6) is obtained as follows:

$$\frac{dy_n(t)}{dt} = \frac{dp_n(t)}{dt} - V(\tilde{s}). \tag{7}$$

Then, the derivative of Equation (7) is obtained as follows:

$$\frac{d^2y_n(t)}{dt^2} = \frac{dv_n(t)}{dt}. \tag{8}$$

The headway can be written as follows:

$$\begin{aligned} s &= p_{n+1}^{(0)}(t) + y_{n+1}(t) - p_n^{(0)}(t) - y_n(t) \\ &= \tilde{s} + \Delta y_n(t). \end{aligned} \tag{9}$$

Substituting the above results into Equation (3), the differential equation of perturbation can be obtained.

$$\begin{aligned} \frac{dy_n^2(t)}{dt^2} &= a\left(V(\tilde{s} + \Delta y_n(t)) - \frac{dp_n(t)}{dt}\right) + \kappa\frac{d^2\Delta y_n(t)}{dt^2} \\ &\quad - (\lambda\Theta(s_c - s) + \gamma)\left(\frac{d^2y_n(t)}{dt^2} - \frac{d^2y_n(t-1)}{dt^2}\right). \end{aligned} \tag{10}$$

By performing a Taylor expansion on Equation (10) and ignoring high-order terms, we can obtain:

$$\begin{aligned} \frac{dy_n^2(t)}{dt^2} &= a\left(V'(\tilde{s})\Delta y_n(t) - \frac{dy_n(t)}{dt}\right) + \kappa\frac{d^2y_n(t)}{dt^2} \\ &\quad - (\lambda\Theta(s_c - s) + \gamma)\left(\frac{d^2y_n(t)}{dt^2} - \frac{d^2y_n(t-1)}{dt^2}\right), \end{aligned} \tag{11}$$

where $\Delta y_n(t) = y_{n+1}(t) - y_n(t)$ and $V'(\tilde{s}) = dV(s)/dt\big|_{s=\tilde{s}}$. Expanding $y_n(t) = \exp(ikn + zt)$ results in:

$$z^2 = a\left(V'\left(e^{ik} - 1\right) - z\right) + (\lambda\Theta(s_c - s) + \gamma)z^2 - \kappa\left(z^2\left(1 - e^{-z}\right)\right). \tag{12}$$

By expanding z in Equation (12) as $z = z_1(ik) + z_2(ik)^2 + \ldots$, we can obtain the following first- and second-order terms of ik:

$$z_1 = V'(\tilde{s}),\ z_2 = \frac{V'}{2} - \left(1 - (\lambda\Theta(s_c - s) + \gamma)\right)\frac{V'^2}{a}. \tag{13}$$

If z_2 is negative, then the traffic flow becomes unstable; if z_2 is positive, then the initial small perturbation in traffic flow vanishes over time. Therefore, the neutral stability condition is given as

$$a = \left(1 - (\lambda\Theta(s_c - s) + \gamma)\right)\frac{V'}{2}. \tag{14}$$

3.2. Nonlinear Stability Analysis. To analyze the slow-varying behavior around the critical point (s_c, a_c) for a coarse grain size, the reductive perturbation method is applied to deduce the mKdV equation, which is inferred to depict the propagation characteristics of traffic jams. By introducing slow scales for space variable n and time variable t, the slowly varying behavior of long waves is studied, and the corresponding slow variables X and T are given as follows:

$$X = \zeta(j + bt),\ T = \zeta^3 t,\quad 0 < \zeta \le 1, \tag{15}$$

where $0 < \varepsilon \le 1$ and b is a to-be-determined constant. The headway $\Delta x_n(t)$ can be followed by $h_c + \varepsilon R(X, T)$. According to Equation (3), the expression of the car-following behavior of the preceding vehicle can be obtained as follows:

$$\begin{aligned} \frac{dv_{n+1}(t)}{dt} &= a\left(V(s_{n+1}) - v_{n+1}(t)\right) + \kappa\Delta v_{n+1}(t) \\ &\quad - (\lambda\Theta(s_c - s) + \gamma)\left(\frac{dv_{n+1}(t)}{dt} - \frac{dv_{n+1}(t-1)}{dt}\right). \end{aligned} \tag{16}$$

By subtracting Equation (3) from Equation (16), we obtain the following form:

$$\begin{aligned} \frac{d^2s_n(t)}{dt^2} &= a\left(V(s_{n+1}(t)) - V(s_n(t)) - \frac{ds_n(t)}{dt}\right) + \kappa\frac{d^2s_n(t)}{dt^2} \\ &\quad - (\lambda\Theta(s_c - s) + \gamma)\left(\frac{d^2s_n(t)}{dt^2} - \frac{d^2s_n(t-1)}{dt^2}\right). \end{aligned} \tag{17}$$

By substituting Equation (15) into Equation (17) and expanding Equation (17) to the fifth order of ζ by taking the Taylor expansion, a nonlinear differential equation is obtained as follows:

$$\begin{aligned} &\zeta^2 g_1\partial_X R + \zeta^3 g_2\partial_X^2 R + \zeta^4\left(g_3\partial_X^3 R + g_4 V'''\partial_X R^3 - \partial_T R\right) \\ &\quad + \zeta^5\left(g_5\partial_X^4 R + g_6\partial_X^2 R^3 + g_7\partial_X\partial_T R\right) = 0, \end{aligned} \tag{18}$$

where $V' = dV(s)/ds|_{s=s_c}$ and $V''' = d^3V(s)/ds^3\big|_{s=s_c}$. By taking $b = V'$ and $a = a_c/\left(1 + \zeta^2\right)$, from Equation (18), we obtain the following simplified equation:

$$\zeta^4\left(g_1\partial_X^3 R + g_2\partial_X R^3 - \partial_T R\right) + \zeta^5\left(g_3\partial_X^4 R + g_4\partial_X^2 R^3 + g_5\partial_X^2\right) = 0, \tag{19}$$

where

$$\begin{aligned} g_1 &= \frac{1}{6}V' - \frac{2(\gamma + \lambda\Theta(s_c - s))V'^4}{1 - \kappa},\ g_2 = \frac{1}{6}V''', \\ g_3 &= \frac{1}{24}V' + \frac{\kappa V'^5}{1 - \gamma - \lambda\Theta(s_c - s)},\ g_4 = \frac{1}{12},\ g_5 = -2V'^3. \end{aligned} \tag{20}$$

By transforming $T = T'/g_i$ and $R = \sqrt{g_1/g_2}$ for Equation (19), the regularized mKdV equation with a corrective term $o(\zeta)$ is obtained as:

$$\partial_{T'}R' = \partial_X^3 R' - \partial_X R'^3 - \zeta\left(\frac{g_3}{g_1}\partial_X^2 R' + \frac{g_4}{g_1}\partial_X^4 R' + \frac{g_5}{g_2}\partial_X^2 R'^3\right). \tag{21}$$

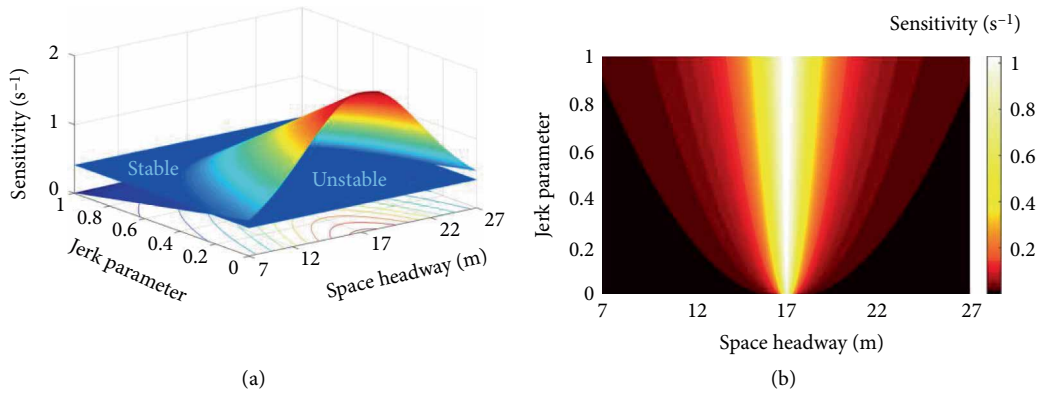

(a) (b)

Figure 4: Stability phase diagram. (a) Neutral stable space. (b) Coexisting phase diagram.

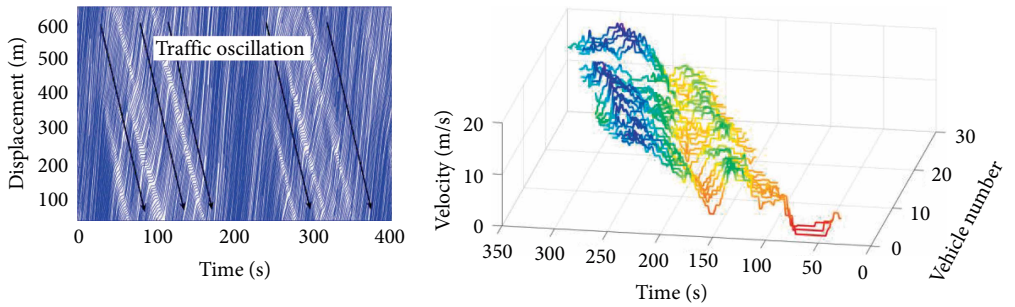

(a) (b)

Figure 5: The traffic flow oscillation observed in the NGSIM dataset. (a) Temporal-spatial trajectories of vehicles. (b) Velocity oscillation wave in a 30-vehicle platoon.

The traffic congestion transition can be described by the mKdV equation with a propagating solution. Using the method in [19, 20], we obtain a kink–antikink soliton solution of the regularized mKdV equation as follows:

$$R_o'(X,T') = \sqrt{c}\tanh\sqrt{\frac{c}{2}}(X - cT'), \tag{22}$$

where c is the spread velocity of the kink–antikink soliton solution. To obtain the spread velocity c, it is necessary for $R_0'(X,T')$to satisfy the following solvability property: $(R_o', M[R_o']) \equiv \int_{-\infty}^{+\infty} dX' R_0' M[R']\}$where $M[R_o'] = (g_3)/(g_1)\partial_X^2 R' + (g_4)/(g_1)\partial_X^4 R' + (g_5)/(g_2)\partial_X^2 R'^3$. We then obtain the spread velocity c of the kink–antikink density wave as follows:

$$c = \frac{5g_2g_3}{2g_2g_4 - 3g_1g_5}. \tag{23}$$

The general density wave solution of the headway is then given by:

$$s_n(t) = s_c \pm \sqrt{\frac{g_1 c}{g_2}\left(\frac{a_c}{a} - 1\right)} \times \tanh\sqrt{\frac{c}{2}\left(\frac{a_c}{a} - 1\right)} \times \left[n + (1 - cg_1)\left(\frac{a_c}{a} - 1\right)t\right]. \tag{24}$$

The kink–antikink soliton solution denotes the coexisting phase. The headway in the freely moving phase is $s = C_1/C_2 + \sqrt{g_1 c(a_c/a - 1)/g_2}$ and that in the congested phase is $s = C_1/C_2 - \sqrt{g_1 c(a_c/a - 1)/g_2}$.

According to Equations (14) and (24), the traffic flow stability distribution is shown in Figures 4(a) and 4(b), respectively. In Figure 4(a), the space above the neutral stable surface is the stable space, and the space below is the unstable space. The stability of the model is improved when considering the jerk effect. Figure 4(b) shows the nonlinear analysis results obtained by the mKdV equation. It can be seen that the jerk effect plays an important role in traffic flow stability and traffic congestion in a connected environment. Notably, the communication transmission delay is equivalent to increasing the reaction delay during driving, which decreases the value of a in the model. According to the stability analysis results shown in Figure 4, a decrease in a will increase the unstable area of traffic flow, which is not conducive to suppressing traffic congestion.

4. Simulation Experiments

The stability of the model affects traffic flow oscillation propagation, which is a common phenomenon on real roads. Figure 5(a) plots the temporal-spatial trajectories of vehicles on Lane 1 of U.S. Highway 101, selected from the Next Generation Simulation (NGSIM) dataset. More specifically, Figure 5(b) plots the propagation of the velocity oscillation wave in a 30-vehicle platoon with the No. 9 vehicle as the leading vehicle. Figure 5 shows that the content of the stability analysis of the previous section is a traffic phenomenon that exists in a real road environment. Therefore, the model we proposed should first be able to reproduce this traffic phenomenon in the next simulation experiment to verify the validity of the model and the premise of making predictions based on the model.

Figure 6: A diagram of the experimental setup.

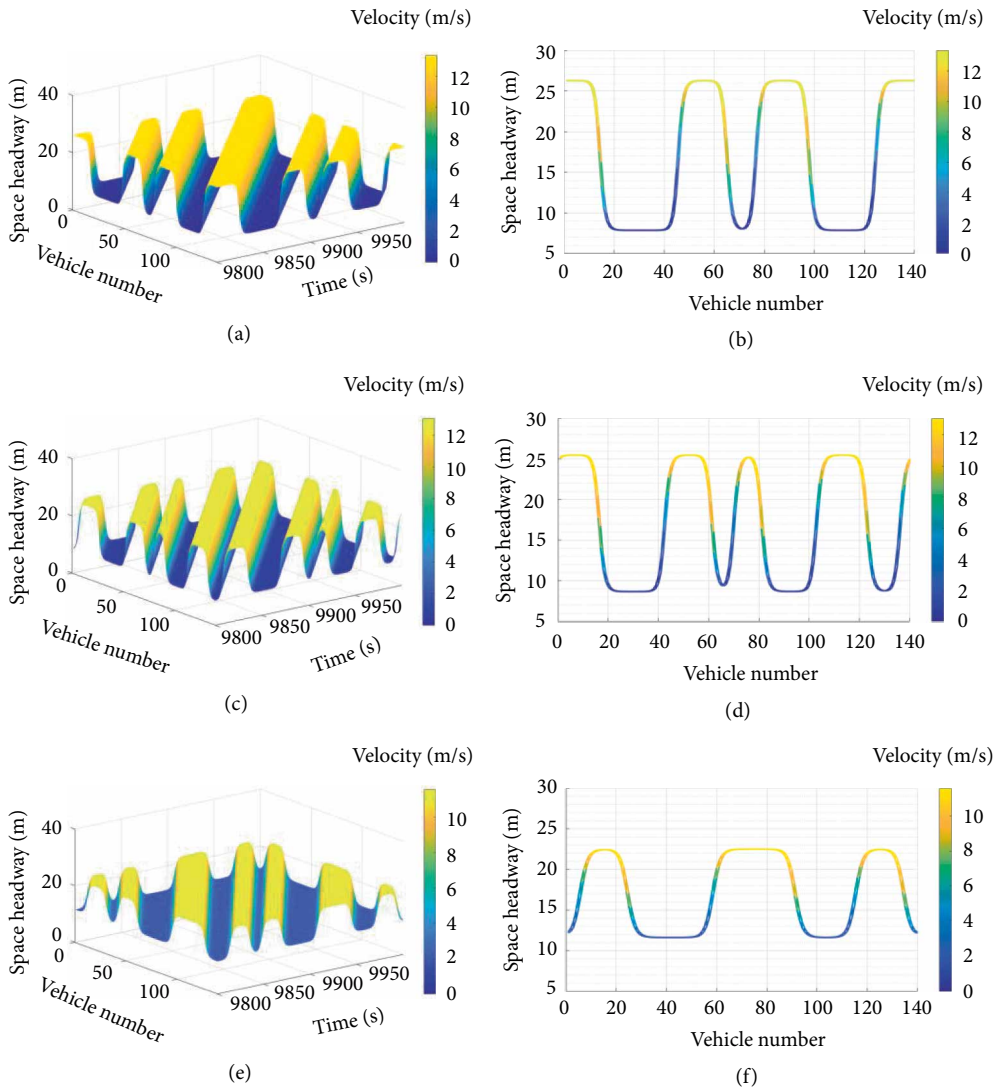

Figure 7: Spatiotemporal evolution of traffic waves under different scenarios. (a) FVD Model. (b) Snapshot at $t = 10{,}000$ corresponding to Pattern (a). (c) Inactive V2V communications. (d) Snapshot at $t = 10{,}000$ corresponding to Pattern (c). (e) Active V2V communications. (f) Snapshot at $t = 10{,}000$ corresponding to Pattern (e).

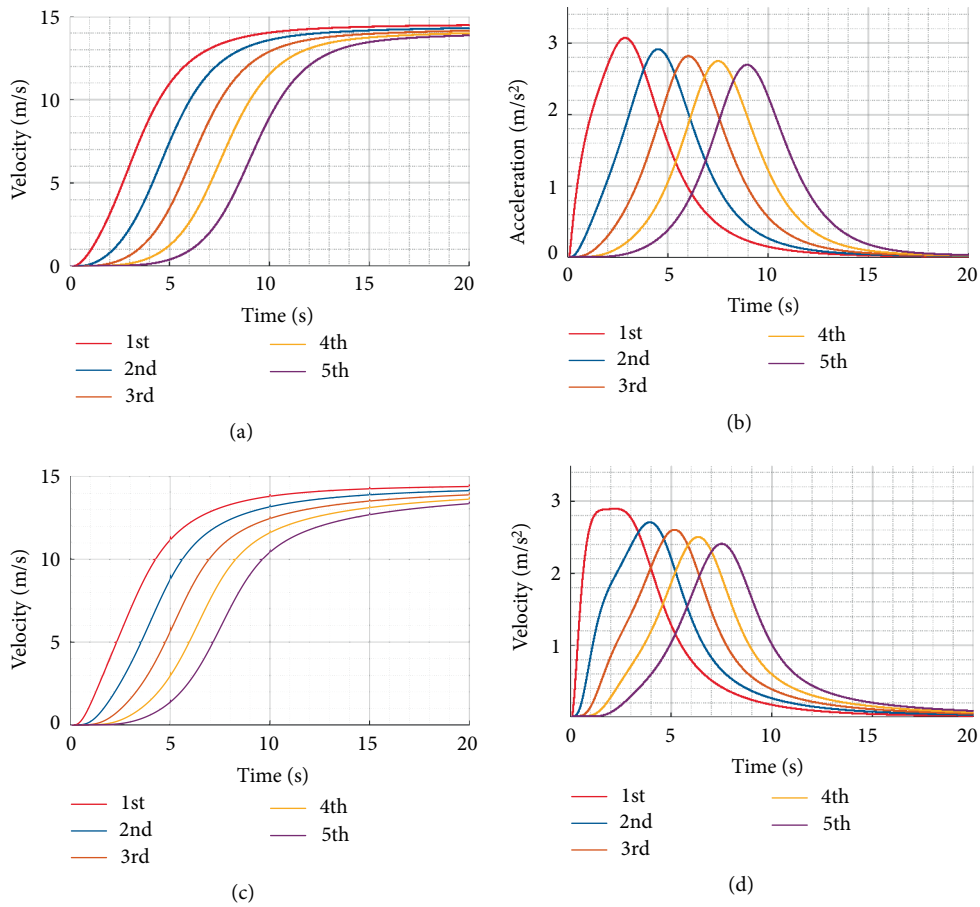

Figure 8: Simulation experiments of the starting process. (a) Velocities of the 5 vehicles simulated by the FVD model. (b) Accelerations of the 5 vehicles simulated by the FVD model. (c) Velocities of the 5 vehicles simulated by the FVD-JC model. (d) Accelerations of the 5 vehicles simulated by the FVD-JC model.

Because the experimental costs and technical requirements are too high on the open road, we set up an equivalent experiment, as shown in Figure 6. The scenario is set as 140 vehicles running in a circular track in the vehicle testing field of Chang'an University. This paper conducts simulation experiments under this traffic scenario only. Field experiments will be conducted in the future. The specifications and assumptions of the simulation system settings are summarized as follows:

(1) The simulation experiments of the CVs are carried out under homogeneous traffic flow, i.e., 100% MPR of the CVs.
(2) During the experiment, it is assumed that communication transmission is reliable and accurate.
(3) The communication transmission delay and the driving response delay are uniformly described by the sensitivity coefficient of the driver's response in vehicle dynamics modeling.

Figure 7 shows the spatiotemporal evolution of traffic oscillation waves in different traffic scenarios. Figure 7(a) presents the traffic flow fluctuation propagation of the traditional FVD model. Figure 7(c) displays a time-space evolution diagram of traffic flow considering the jerk effect without activating V2V communication. The amplitude of the headway and the velocity fluctuations are smaller than those in Figure 7(a). Figure 7(e) shows traffic oscillation propagation after V2V communication is activated. The stability of the traffic flow is improved compared to that shown in Figure 7(c). Figures 7(b), 7(d) and 7(f) illustrate snapshots corresponding to Figures 7(a), 7(c) and 7(e) when $t = 1000$ s, respectively. The experimental results are consistent with the theoretical analysis.

To further compare the FVD model and the FVD-JC model, we conducted simulation experiments of the starting and braking process processes of a 5-vehicle platoon.

The starting process simulates the start of the platoon after a traffic signal turns from red to green. At the initial moment of the simulation, the position of each vehicle is $x_n(0) = (n-1)\Delta x_n$, where $n = 1, 2, ..., 5$ and the headway $\Delta x_n = 7.5$ m. All vehicles are at rest, i.e., $v_n(0) = 0$ m/s. Then, the first vehicle starts, and each vehicle starts in turn. According to the vehicle motion delay, the kinematic wave velocity at the jam density can be estimated by $c_j = \Delta x_n/\delta t$. The values of c_j of the FVD model and the FVD-JC model are 17.8 km/h and 22.2 km/h, respectively. The kinematic wave velocity of the FVD-JC model is significantly higher than that of the FVD model, indicating that the FVD-JC model enables the platoon to start in a shorter time. The velocity and acceleration profiles

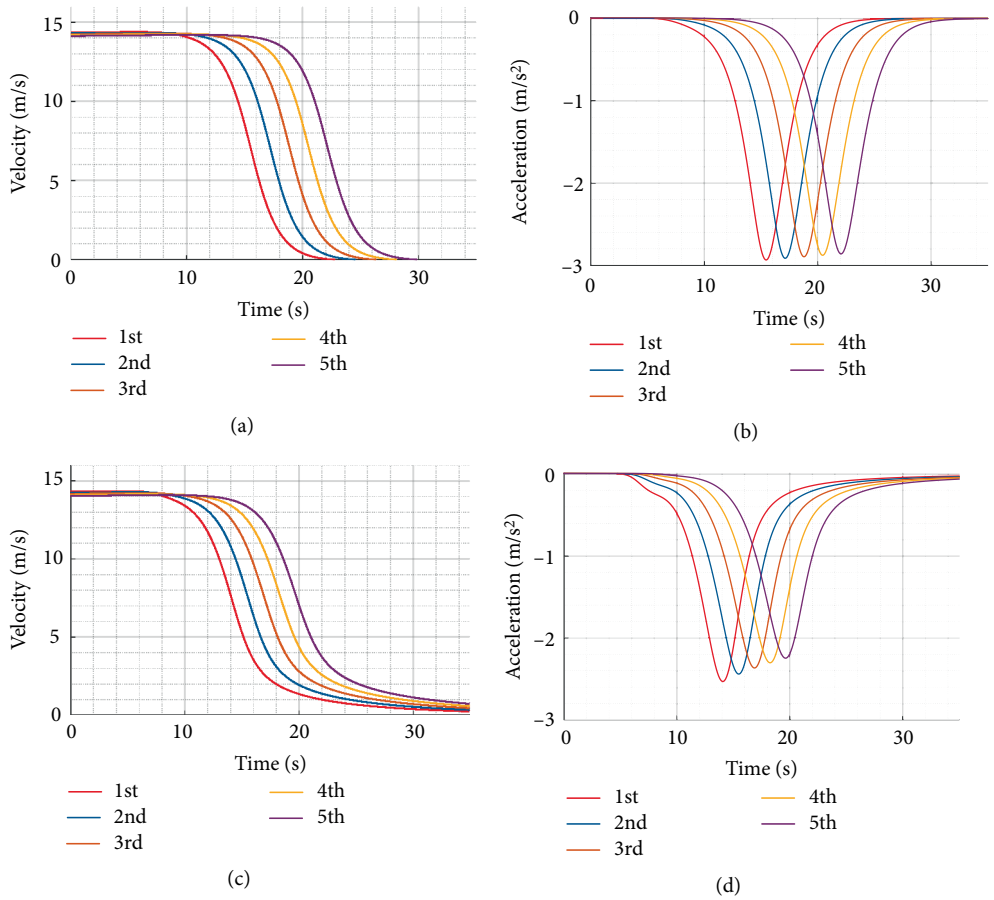

Figure 9: Simulation experiments of the braking process. (a) Velocities of the 5 vehicles simulated by the FVD model. (b) Accelerations of the 5 vehicles simulated by the FVD model. (c) Velocities of the 5 vehicles simulated by the FVD-JC model. (d) Accelerations of the 5 vehicles simulated by the FVD-JC model.

of the FVD model and the FVD-JC model during the starting process of the platoon are shown in Figure 8.

Figures 8(a) and 8(b) show that the convergence rate of the FVD-JC model reaching the desired velocity of the platoon is faster than that of the FVD model. This result indicates that the FVD-JC model takes less time to bring the entire platoon to a steady state during the vehicle starting process. Figures 8(c) and 8(d) show that the peak value of the acceleration of the FVD-JC model is smaller than that of the FVD model during the starting process. This result indicates that the starting process of the FVD-JC model is smoother and more comfortable than that of the FVD model. Therefore, the FVD-JC model can achieve the desired velocity in a shorter time with a smoother and more comfortable start of the platoon than the FVD model.

The simulation scene of the braking process is set as follows. A 5-vehicle platoon runs at a constant velocity of 14.36 m/s. There is a stop line at 31 m in front of the first vehicle of the platoon, and the traffic signal turns red at this time. Figure 9 depicts the velocity and acceleration changes in the FVD model and the FVD-JC model during the stop process.

The results of Figures 9(a) and 9(b) show that the FVD-JC model can complete the stop process in a shorter time than the FVD model. Figures 9(c) and 9(d) show that the amplitude of deceleration is reduced in the FVD-JC model compared with the FVD model. This finding indicates that the FVD-JC model decelerates more smoothly during the stop process than the FVD model. Therefore, the platoon of the FVD-JC model can stop in a shorter time with a more comfortable brake than the FVD model.

5. Conclusions

Using the car-following data of CVs previously collected by our research team in the vehicle testing field of Chang'an University, this paper uses the MIC to analyze the correlation between the jerk effect and car-following behavior under inactive and active V2V environments. The data mining results show that the correlation between the jerk effect and driving behavior increases in a connected environment, as V2V communication technology provides instant information interaction between vehicles. To better reproduce the experimental results and capture the nature of the jerk effect in a connected environment, a car-following model is proposed based on the data analysis results. The GA is used to calibrate the model parameters. The calibration results show that the standard deviation between the FVD-JC model simulation data and the observed data is reduced by 38.2% compared to that of the

FVD model. Therefore, the extension of the FVD model is effective and meaningful. It is more reasonable to use the FVD-JC model to analyze the jerk effect in connected traffic flow than the FVD model.

Linear and nonlinear stability analyses of the calibrated FVD-JC model are then carried out to analyze the connected traffic flow stability and the corresponding slow-change characteristics near the critical point. The theoretical analysis results show that the jerk effect plays an important role in the traffic flow stability and traffic congestion. Finally, the theoretical analysis is verified by setting up a simulation experiment of 140 vehicles running on the loop of the vehicle testing field of Chang'an University. The simulation results show that the amplitude of the headway and the velocity fluctuations are reduced when considering the jerk effect in a connected environment, and the stability of traffic flow is improved. The simulation experiment results are in good agreement with the theoretical analysis.

The research results can be used for microscopic traffic flow simulation, thus providing accurate and reasonable traffic planning recommendations for traffic management departments. This research is also helpful for the design of upper-level control strategies for human-like autonomous vehicles. In the future, we will collect more field data and investigate the jerk effect under heterogeneous traffic flow in a connected environment.

Data Availability

The full US 101 dataset is freely available at the NGSIM website at https://ops.fhwa.dot.gov/trafficanalysistools/ngsim.htm. The car-following data of CVs used to support the findings of this study may be released upon request to the Joint Laboratory for Internet of Vehicles, Ministry of Education—China Mobile Communications Corporation, who can be contacted at 86-29-82334763.

Conflicts of Interest

The authors declare that they have no conflicts of interest regarding the publication of this paper.

Acknowledgments

This study was supported by the National Key R&D Program of China (Grant Nos. 2017YFC0804806 and 2018YFB160060403), the National Natural Science Foundation of China (Grant No. 61603058), the 111 Project (Grant No. B14043), the Joint Laboratory of Internet of Vehicles sponsored by the Ministry of Education and China Mobile (Grant No. 213024170015), the Key R&D Program of Shaanxi Province (Grant Nos. 2018ZDCXL-GY-04-02 and 2018ZDCXL-GY-05-01), and the Fundamental Research Funds for the Central Universities (Grant Nos. 300102248301 and 300102249503). The first author is grateful for the financial support of the China Scholarship Council (CSC).

References

[1] H. Zhao, R. He, and C. Ma, "An extended car-following model at signalised intersections," *Journal of Advanced Transportation*, vol. 2018, Article ID 5427507, 26 pages, 2018.

[2] M. Seraj, J. Li, and Z. Qiu, "Modeling microscopic car-following strategy of mixed traffic to identify optimal platoon configurations for multiobjective decision-making," *Journal of Advanced Transportation*, vol. 2018, Article ID 7835010, 15 pages, 2018.

[3] L. Zheng, C. Zhu, Z. B. He, T. He, and S. S. Liu, "Empirical validation of vehicle type-dependent car-following heterogeneity from micro- and macro-viewpoints," *Transportmetrica B: Transport Dynamics*, vol. 7, no. 1, pp. 765–787, 2019.

[4] J. J. Zhang, Y. P. Wang, and G. Q. Lu, "Impact of heterogeneity of car-following behavior on rear-end crash risk," *Accident Analysis and Prevention*, vol. 125, pp. 275–289, 2019.

[5] N. F. Wan, C. Zhang, and A. Vahidi, "Probabilistic anticipation and control in autonomous car following," *IEEE Transactions on Control Systems Technology*, vol. 27, no. 1, pp. 30–38, 2019.

[6] M. Bando, K. Hasebe, A. Nakayama, A. Shibata, and Y. Sugiyama, "Dynamical model of traffic congestion and numerical simulation," *Physical Review E: Statistical Physics Plasmas Fluids & Related Interdisciplinary Topics*, vol. 51, no. 2, pp. 1035–1042, 1995.

[7] D. Helbing and B. Tilch, "Generalized force model of traffic dynamics," *Physical Review E: Statistical Physics Plasmas Fluids & Related Interdisciplinary Topics*, vol. 58, no. 1, pp. 133–138, 1998.

[8] R. Jiang, Q. Wu, and Z. Zhu, "Full velocity difference model for a car-following theory," *Physical Review E*, vol. 64, no. 1, Article ID 017101, 2001.

[9] Y. Li, Z. Zhong, K. Zhang, and T. Zheng, "A car-following model for electric vehicle traffic flow based on optimal energy consumption," *Physica A: Statistical Mechanics and its Applications*, vol. 533, Article ID 122022, 2019.

[10] D. Jia, D. Ngoduy, and H. L. Vu, "A multiclass microscopic model for heterogeneous platoon with vehicle-to-vehicle communication," *Transportmetrica B: Transport Dynamics*, vol. 7, no. 1, pp. 448–472, 2019.

[11] X. Chang, H. Li, J. Rong, Z. Huang, X. Chen, and Y. Zhang, "Effects of on-board unit on driving behavior in connected vehicle traffic flow," *Journal of Advanced Transportation*, vol. 2019, Article ID 8591623, 12 pages, 2019.

[12] D. Jia, D. Ngoduy, and H. L. Vu, "A multiclass microscopic model for heterogeneous platoon with vehicle-to-vehicle communication," *Transportmetrica B: Transport Dynamics*, vol. 7, no. 1, pp. 448–472, 2018.

[13] Y. F. Li, C. C. Tang, S. Peeta, and Y. B. Wang, "Integral-sliding-mode braking control for a connected vehicle platoon: theory and application," *IEEE Transactions on Industrial Electronics*, vol. 66, no. 6, pp. 4618–4628, 2019.

[14] R. M. Jannes, C. Melson, J. Hu, and J. Bared, "Characterizing the impact of production adaptive cruise control on traffic flow: an investigation," *Transportmetrica B: Transport Dynamics*, vol. 7, no. 1, pp. 992–1012, 2019.

[15] Y. Li, C. Tang, K. Li, X. He, S. Peeta, and Y. Wang, "Consensus-based cooperative control for multi-platoon under the connected vehicles environment," *IEEE Transactions on Intelligent Transportation Systems*, vol. 20, no. 6, pp. 2220–2229, 2019.

[16] Y. Li, C. Tang, S. Peeta, and Y. Wang, "Nonlinear consensus-based connected vehicle platoon control incorporating car-following interactions and heterogeneous time delays," *IEEE Transactions on Intelligent Transportation Systems*, vol. 20, no. 6, pp. 2209–2219, 2019.

[17] Y. F. Li, W. B. Chen, S. Peeta, and Y. Wang, "Platoon control of connected multi-vehicle systems under v2x communications: design and experiments," *IEEE Transactions on Intelligent Transportation Systems*, pp. 1–12, 2019.

[18] J. I. Ge, S. S. Avedisov, C. R. He, W. B. Qin, M. Sadeghpour, and G. Orosz, "Experimental validation of connected automated vehicle design among human-driven vehicles," *Transportation Research Part C: Emerging Technologies*, vol. 91, pp. 335–352, 2018.

[19] D. F. Xie, X. M. Zhao, and Z. B. He, "Heterogeneous traffic mixing regular and connected vehicles: modeling and stabilization," *IEEE Transactions on Intelligent Transportation Systems*, vol. 20, no. 6, pp. 2060–2071, 2018.

[20] A. Sharma, Z. Zheng, A. Bhaskar, and M. M. Haque, "Modelling car-following behaviour of connected vehicles with a focus on driver compliance," *Transportation Research Part B: Methodological*, vol. 126, pp. 256–279, 2019.

[21] L. Zheng, C. Zhu, Z. He, and T. He, "Safety rule-based cellular automaton modeling and simulation under V2V environment," *Transportmetrica A: Transport Science*, pp. 1–26, 2018.

[22] Z. J. Wang, S. F. Ma, R. Jiang, and J. F. Tian, "A cellular automaton model reproducing realistic propagation speed of downstream front of the moving synchronized pattern," *Transportmetrica B: Transport Dynamics*, vol. 7, no. 1, pp. 295–310, 2019.

[23] H. Yu and M. Krstic, "Traffic congestion control for Aw-Rascle-Zhang model," *Automatica*, vol. 100, pp. 38–51, 2019.

[24] M. Treiber and A. Kesting, "The intelligent driver model with stochasticity – new insights into traffic flow oscillations," *Transportation Research Part B: Methodological*, vol. 117, pp. 613–623, 2018.

[25] P. Redhu and V. Siwach, "An extended lattice model accounting for traffic jerk," *Physica A: Statistical Mechanics and its Applications*, vol. 492, pp. 1473–1480, 2018.

[26] C. Zhai and W. T. Wu, "Analysis of drivers' characteristics on continuum model with traffic jerk effect," *Physics Letters A*, vol. 382, no. 47, pp. 3381–3392, 2018.

[27] R. J. Cheng, H. X. Ge, and J. F. Wang, "The nonlinear analysis for a new continuum model considering anticipation and traffic jerk effect," *Applied Mathematics and Computation*, vol. 332, pp. 493–505, 2018.

[28] H. Song, H. X. Ge, F. Z. Chen, and R. J. Cheng, "TDGL and mKdV equations for car-following model considering traffic jerk and velocity difference," *Nonlinear Dynamics*, vol. 87, no. 3, pp. 1809–1817, 2017.

[29] Z. Jin, Z. Li, R. Cheng, and H. Ge, "Nonlinear density wave investigation for an extended car-following model considering driver's memory and jerk," *Modern Physics Letters B*, vol. 32, no. 1, Article ID 1750366, 2018.

[30] N. Saxena, T. H. Rashidi, V. V. Dixit, and S. T. Waller, "Modelling the route choice behaviour under stop-&-go traffic for different car driver segments," *Transportation Research Part A: Policy and Practice*, vol. 119, pp. 62–72, 2019.

[31] M. X. Zhu, X. S. Wang, and Y. H. Wang, "Human-like autonomous car-following model with deep reinforcement learning," *Transportation Research Part C: Emerging Technologies*, vol. 97, pp. 348–368, 2018.

[32] Q. Lin, Y. H. Zhang, S. Verwer, and J. Wang, "MOHA: A multi-mode hybrid automaton model for learning car-following behaviors," *IEEE Transactions on Control Systems Technology*, vol. 20, no. 2, pp. 790–796, 2019.

[33] T. Li, F. Hui, and X. Zhao, "An improved car-following model considering the impact of safety messages," *Modern Physics Letters B*, vol. 32, no. 32, p. 1850398, 2018.

[34] X. M. Zhao, S. C. Jing, F. Hui, R. Liu, and A. J. Khattak, "DSRC-based rear-end collision warning system – an error-component safety distance model and field test," *Transportation Research Part C: Emerging Technologies*, vol. 107, pp. 92–104, 2019.

[35] D. N. Reshef, Y. A. Reshef, H. K. Finucane et al., "Detecting novel associations in large data sets," *Science*, vol. 334, no. 6062, pp. 1518–1524, 2011.

[36] Q. Lu and K. D. Kim, "Autonomous and connected intersection crossing traffic management using discrete-time occupancies trajectory," *Applied Intelligence*, vol. 49, no. 5, pp. 1621–1635, 2019.

[37] B. Xu, X. J. Ban, Y. G. Bian et al., "Cooperative method of traffic signal optimization and speed control of connected vehicles at isolated intersections," *IEEE Transactions on Intelligent Transportation Systems*, vol. 20, no. 4, pp. 1390–1403, 2019.

[38] A. Sharma, Z. D. Zheng, and A. Bhaskar, "Is more always better? The impact of vehicular trajectory completeness on car-following model calibration and validation," *Transportation Research Part B: Methodological*, vol. 120, pp. 49–75, 2019.

[39] L. Li, X. Q. Chen, and L. Zhang, "A global optimization algorithm for trajectory data based car-following model calibration," *Transportation Research Part C: Emerging Technologies*, vol. 68, pp. 311–332, 2016.

[40] Y. P. Wang, J. J. Zhang, and G. Q. Lu, "Influence of driving behaviors on the stability in car following," *IEEE Transactions on Intelligent Transportation Systems*, vol. 20, no. 3, pp. 1081–1098, 2019.

[41] H. Wang, Y. Y. Qin, W. Wang, and J. Chen, "Stability of CACC-manual heterogeneous vehicular flow with partial CACC performance degrading," *Transportmetrica B: Transport Dynamics*, vol. 7, no. 1, pp. 788–813, 2019.

[42] J. Sau, J. Monteil, and M. Bouroche, "State-space linear stability analysis of platoons of cooperative vehicles," *Transportmetrica B: Transport Dynamics*, vol. 7, no. 1, pp. 18–43, 2019.

[43] C. Osorio and V. Punzo, "Efficient calibration of microscopic car-following models for large-scale stochastic network simulators," *Transportation Research Part B: Methodological*, vol. 119, pp. 156–173, 2019.